Research Article Vol. 28, No. 4 / 17 February 2020 / Optics Express 5749
Optics EXPRESS

Ge-on-Si waveguides for sensing in the molecular fingerprint regime

UGNE GRISKEVICIUTE,[1,2] ROSS W. MILLAR,[1,2] KEVIN GALLACHER,[1] JOAO VALENTE,[1] AND DOUGLAS J. PAUL[1,*]

[1] University of Glasgow, James Watt School of Engineering, Rankine Building, Oakfield Avenue, Glasgow G12 8LT, UK
[2] These authors contributed equally to the work
[*] Douglas.Paul@glasgow.ac.uk

Abstract: Low loss, single mode, Ge-on-Si rib waveguides are used to demonstrated optical sensing in the molecular fingerprint region of the mid-infrared spectrum. Sensing is carried out using two spin-coated films, with strong absorption in the mid-infrared. These films are used to calibrate the modal overlap with an analyte, and therefore experimentally demonstrate the potential for Ge-on-Si waveguides for mid-infrared sensing applications. The results are compared to Fourier transform infrared spectroscopy measurements. The advantage of waveguide spectroscopy is demonstrated in terms of the increased optical interaction, and a new multi-path length approach is demonstrated to improve the dynamic range, which is not possible with conventional FTIR or attenuated total reflection (ATR) measurements. These results highlight the potential for Ge-on-Si as an integrated sensing platform for healthcare, pollution monitoring and defence applications.

1. Introduction

The mid-infrared (MIR) spectral region is of significant interest for establishing on-chip spectroscopy; particularly in the spectral region between 6.7 and 20 μm wavelength, as the unique molecular vibration modes allow for a label free sensing platform [1]. This region is known as the 'molecular fingerprint' region. Such sensing is of particular interest for a number of growing markets including health-care [1], environmental monitoring [2,3], chemical biomolecular sensing [4], forensic analysis [5,6] and security applications [7,8]. All of these sectors and applications would benefit from a low-cost, small footprint sensing platform to enable wide-spread uptake for rapid feedback and analysis outside of the laboratory. The current gold standard for infrared identification of unknown analytes is Fourier transform infrared (FTIR) spectroscopy, which is expensive, bulky and requires significant expertise for successful operation [5].

A number of on-chip optical sensing devices have been fabricated using Si, which are low loss in the near-IR (NIR) part of the spectrum, however, while these NIR devices can be highly sensitive, they typically rely on the refractive index shift caused by an analyte to detect its presence, in the absence of strong absorption lines. This allows for molecular identification only when the waveguide surface is treated with a surfactant to promote binding to a particular molecule, as a number of analytes have comparable refractive indices.

For operation in the MIR, alternate materials with wider transparency windows have been investigated, such as chalcogenide glasses [9], group III-V materials (GaAs and InSb) [10] and silver halides [11]. Ge has also been proposed as a platform for MIR sensing, due its transparency up to ~15 μm. Various compositions of Ge in SiGe materials have been investigated on SiGe graded buffers [12], as well as Ge-on-nothing [13] and Ge-on-insulator [14]. The Ge-on-SiN material systems can provide low loss and tight bending radii in the 3-5 μm regime [15] but

#382356 https://doi.org/10.1364/OE.382356
Journal © 2020 Received 6 Nov 2019; revised 31 Jan 2020; accepted 3 Feb 2020; published 14 Feb 2020

Optics EXPRESS

are limited to wavelenghts ≤ 7 μm due to strong absorption from the Si-N bond. A number of Ge-on-Si components have been demonstrated to enable photonic integrated circuits for chip-scale MIR sensing in the important fingerprint region including quantum well infrared photodetection [16], plasmonic antenna enhancement of molecular absorptions [8], and third harmonic generation [17].

Here, we demonstrate waveguide spectroscopy using low loss Ge-on-Si rib waveguides in the molecular fingerprint regime, and use spin coated films with measured absorption coefficients in order to experimentally calibrate the optical overlap and predict the potential performance of complete systems. Waveguide spectroscopy can provide improved sensitivity compared to techniques such as attenuated total reflectance (ATR) FTIR, as rather than discrete reflections, a continuous evanescent wave can interact with an analyte. There is therefore significant scope for chip-scale waveguide systems to be used as evanescent sensing elements as part of integrated MIR sensing chips. Such broadband low losses, coupled with extremely strong molecular absorption, can allow for unique spectral identification; for example, home-made explosives like tri-acetone tri-peroxide (TATP) [7] and bioweapons including mustards [8,18] and VX [19] have unique absorption lines in the ~7 to 15 μm sensing window. Furthermore, spectroscopic analysis of proteins from spinal fluid can reveal the early onset of neurodegenerative diseases [20]. Sensing of proteins has recently been demonstrated with multi-mode Ge-on-Si waveguides [21]. SiGe waveguide sensing has also been demonstrated at wavelengths below the molecular fingerprint region [6], and demonstrated modal power overlaps of ~ 0.61 % with the analyte.

For waveguide spectroscopy, the key figures of merit relevant to the waveguide sensing element are the optical loss and modal overlap with the analyte, which define the maximum effective interaction length. Group IV material systems will benefit significantly from low production costs and compatability with Si foundry processing, however to date there has been no experimental calibration of the sensing performance of Group IV waveguides within the molecular fingerprint regime (6.7 to 20 μm). Furthermore, we demonstrate a unique benefit of waveguide spectroscopy, by using a multi-path length geometry to effectively improve the dynamic range of the measurement, allowing the observation of both strong and weak absorption lines. This is a key factor for identification, and an issue with ATR spectroscopy, which requires various crystals to be changed to reduce or enhance the analyte interaction length accordingly.

2. Fabrication and measurement

The Ge rib waveguides were fabricated using commercially available material (IQE Si, details in [22]). The waveguides were patterned by electron-beam lithography by using hydrogen silsesquioxane (HSQ) resist. They were subsequently etched by 1.25 μm in a SF_6 and C_4F_8 recipe [23]. Residual HSQ was removed using dilute hydrofluoric acid (HF), and then diced using a diamond saw and polished to form optically smooth facets. For sensing measurements the samples were spin-coated with either a polymer or an inorganic compound, both of which have strong absorption lines in the MIR. In particular, polymethyl methacrylate (PMMA) and HSQ were used to observe molecular vibrations at different wavelengths in the molecular fingerprint regime. Initially, 4 μm wide waveguides were spin coated with PMMA. The polymer was patterned using a shadow mask, and etched using an oxygen plasma ash, to leave approximately a 1 mm strip coating a waveguide.

Waveguide measurements were undertaken using an external cavity quantum cascade laser (QCL) package emitting from 7.5 to 11.5 μm, which was coupled to the waveguides via a free space optical setup, as described elsewhere [22]. The transmission of each waveguide was measured by stepping the laser wavelength in 10 nm increments and recording the spectra using a liquid nitrogen cooled mercury cadmium telluride (MCT) detector. The modal loss due to the analyte is then calculated using the transmission of bare and coated waveguides. Likewise, surface normal FTIR transmission measurements were obtained from a ~ 40 nm thick PMMA

Optics EXPRESS

film, on a double sided polished float zone (Fz) Si substrate, using a Bruker Vertex 70 FTIR system.

3. Results

3.1. Polymethyl methacrylate

A range of C-O-C stretching bonds can clearly be observed in the spectral region of 7.5 to 9.5 μm wavelength, as demonstrated in Fig. 1. For the surface normal, single pass FTIR measurement, the transmission is reduced to ~ 94 % when the PMMA film has maximum attenuation. The increased attenuation from the waveguide geometry can clearly be observed, with the signal being almost fully attenuated at ~ 8.4 μm. This demonstrates that despite an optical overlap of < 2 %, the waveguide geometry allows for enhanced interaction with the analyte due to the increased optical path length compared to surface normal FTIR measurements. This is particularly appropriate for analysis of proteins and DNA, as surface normal FTIR measurements are dominated by water absorption in the solution, and attenuated total reflection measurements have limited interaction due to a finite number of reflections [24].

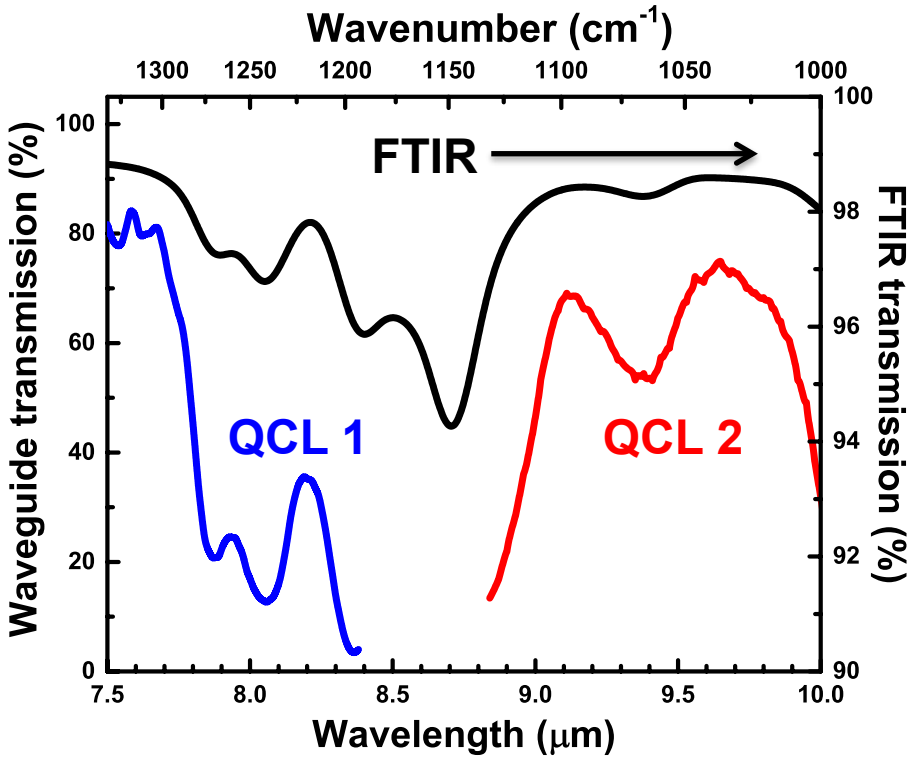

Fig. 1. A transmission measurement of PMMA using both FTIR and waveguide spectroscopy. The black curve is from FTIR, whilst the blue and red curves demonstrate waveguide measurements (from separate QCL lasers).

3.2. Hydrogen silsesquioxane

Further measurements were undertaken using waveguides of widths 3, 4 and 5 μm. In this experiment HSQ, which is a negative electron-beam lithography resist, was used to demonstrate

Optics EXPRESS

and calibrate sensing. Unexposed HSQ was removed by developing in a tri-methyl ammonium hydroxide (TMAH) solution. Given the full attenuation observed with PMMA, a multi-path length approach was patterned in order to increase the dynamic range of the measurement. For each waveguide width, a bare reference waveguide was stripped fully of HSQ and left air-clad (bare), while three further nominally identical waveguides were partially coated by ~ 600 nm thick HSQ (as measured on a planar sample); with HSQ strips of 10 μm, 100 μm and 1000 μm long segments respectively. Figure 2 presents a top down optical image of the waveguides coated with HSQ, and a scanning electron microscope (SEM) image of the air-clad Ge waveguide coated with a 10 μm strip of HSQ.

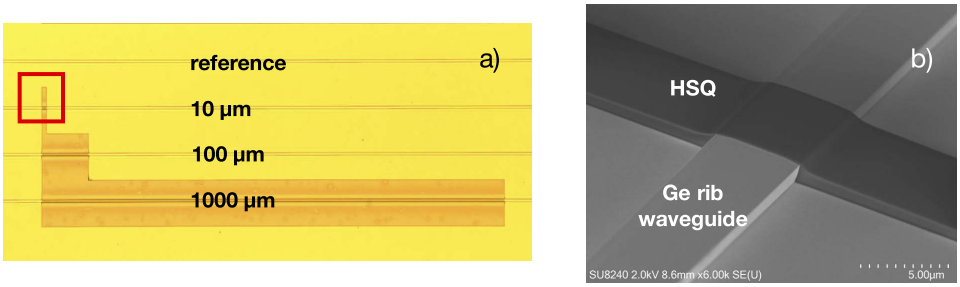

Fig. 2. (a) A top down image of Ge-on-Si rib waveguides, with various lengths of HSQ coatings. (b) A scanning electron microscope image of a Ge-on-Si rib waveguide with a 10 μm section coated with HSQ.

Surface normal FTIR was carried out as described previously, on 115 nm thick, cured HSQ film (thickness measured by ellipsometry). The FTIR transmission was used to calculated the absorption coefficient of the film. In Fig 3(a), a Si-O-Si vibration is clearly visible, which demonstrates an extremely high absorption coefficient of ~ 9.5 $\times 10^5$ dB/cm.

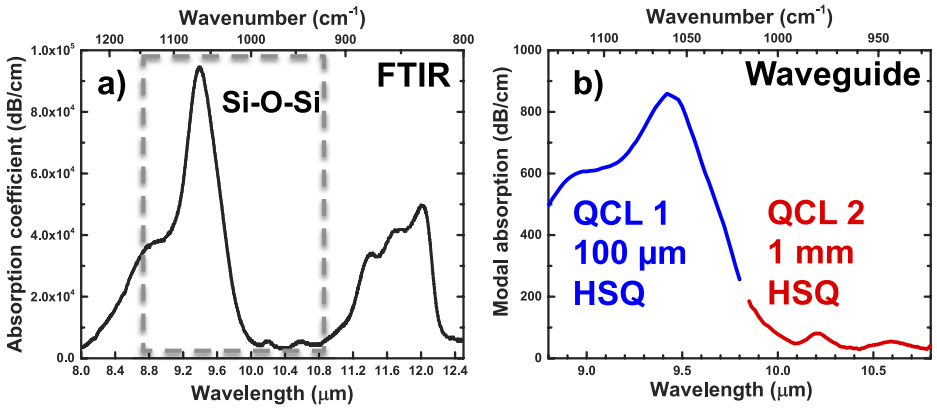

Fig. 3. (a) The absorption coefficient of a thermally cured HSQ film, as measured by FTIR spectroscopy. (b) The modal loss from HSQ films of varying path length, on a 3 μm wide Ge-on-Si waveguide in TM polarisation.

For the waveguide measurement, the extracted absorption coefficient is the modal absorption coefficient from the analyte (i.e. the analyte loss experienced by the mode per cm of propagation). The waveguide measurements presented here are in transverse magnetic (TM) polarisation. The results are demonstrated in Fig. 3(b). In the range 8.8 to 9.8 μm, the strong Si-O-Si vibrations can be observed. As the film is exposed to high energy electrons, or cured thermally, the molecular

Optics EXPRESS

structure is modified from 'cage-like' to 'network-like' [25], and the Si-O-Si bond absorption red-shifts from ~ 8.8 to 9.4 μm wavelength. For both thermally cured, and electron-beam written films, a shoulder is present at 8.8 μm, with the dominant peak at ~ 9.4 μm, indicating the film is approaching a network structure. In the waveguide geometry, this vibration was measured using a 100 μm path length. Full attenuation was observed for this bond in the 1 mm path, meaning it could not be measured using the longest HSQ region. Two further peaks are observed at ~ 10.2 μm (981 cm^{-1}) and ~ 10.57 μm (946 cm^{-1}). These peaks have been assigned to the formation of $H_2SiO_{2/2}$ from $HSiO_{3/2}$; a reaction which takes places in the regime of cage-network redistribution with exposure to a high energy electron-beam [25]. These weaker vibrations were measured using a Ge waveguide coated with 1 mm of HSQ. The multi-path length approach allowed the signal to noise ratio (SNR) to be maximised for the given spectral region. This approach could be key for high sensitivity molecular fingerprint identification with analytes containing significant intensity variations in their absorption spectra. In practise, this could be achieved by varying the waveguide propagation length within a fixed length sensing window (i.e. with spiral waveguides). This is a unique feature of waveguide spectroscopy that to our knowledge, has not been demonstrated. With a technique like ATR-FTIR, the entire crystal would have to be changed to modify the interaction length with the analyte.

The SNR enhancement is visible in Fig. 4, which demonstrates the transmission data for a 5 μm wide waveguide, through both 10 μm and 100 μm of HSQ, measured under nominally identical conditions (source power, integration time, etc.). Figure 4(b) presents the resulting modal absorption coefficient for each waveguide. Significant noise is present on the measurement taken with the 10 μm path length.

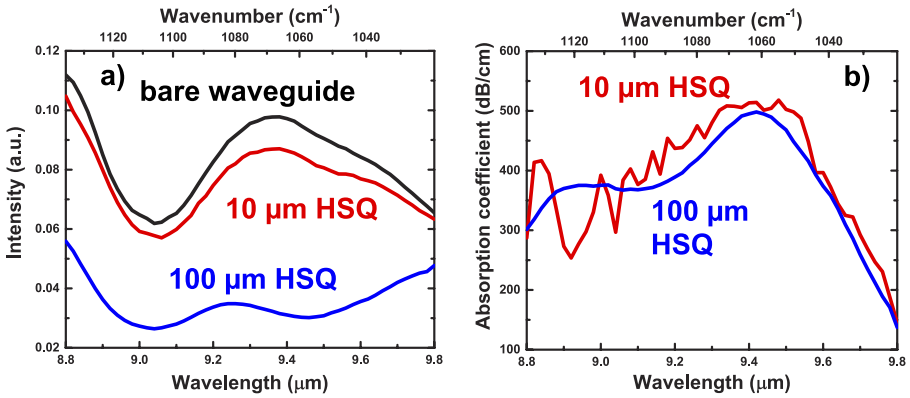

Fig. 4. (a) Transmission measurements of three Ge-on-Si rib waveguides. The first is with no HSQ analyte present (bare), whilst the second and third have sections of the waveguide covered with HSQ (10 μm and 100 μm sections, respectively). (b) The corresponding measured modal absorption coefficients for the coated waveguides. The length of the HSQ coating is labelled on the figure.

The agreement on peak intensity from the two measurements, however, indicates good uniformity of both the waveguide facets and the propagation losses in the waveguides. Misalignment, or any differences in the waveguide losses between the three measured waveguides would result in errors in the calculated absorption coefficient of the analyte but this is not observed.

3.3. Overlap calibration

The modal overlap with the analyte was investigated with varying waveguide widths. Figure 5 demonstrates the measured modal overlaps for 3, 4 and 5 μm wide waveguides, from the Si-O-Si vibration at ~ 9.4 μm. As discussed previously, the intensity/lineshape of this vibration is

Optics EXPRESS

dependant on the level to which the HSQ is cured. The electron-beam written HSQ measured by evanescent waveguide spectroscopy appeared consistent with thin films cured between 400 and 450°C, Fig. 5(a), which were used as upper and lower bounds for estimating the optical overlap in waveguides. This was compared with finite difference eigenmode models (shown as a square in Fig. 5(b), in which the profile of the HSQ over the waveguide was approximated, based on measurements by atomic force microscopy (AFM) (see Fig. 5(c)). The results are in reasonable agreement, however discrepancies may arise from the abrupt change of the film's refractive index close to the Si-O-Si vibration, as well as HSQ thickness variations on the waveguide which have not been accounted for in the model. Notably, the 3 μm wide waveguide has approximately 1.75 to 2.25 % overlap with the analyte in transverse electric (TE) polarisation. This is a conservative estimate for the maximum overlap achievable, as the HSQ films coat only < 100 nm of the top surface for these structures, meaning the evanescent tail decays beyond the analyte, as discussed further in the Discussion section.

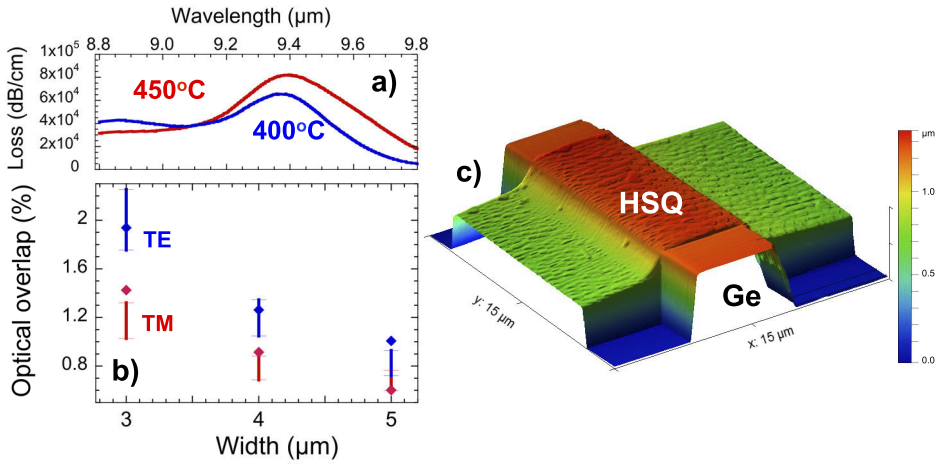

Fig. 5. (a) The measured absorption coefficient of two HSQ films cured at different temperatures. (b) The calculated modal overlaps at 9.4 μm wavelength, based on the measured modal absorptions in waveguides of various widths, and the HSQ absorption coefficient. The upper and lower bounds are calculated using the absorption from part (a). The simulated overlap with the analyte is shown as a square. (c) AFM scan of a Ge waveguide coated by a 10μm strip of HSQ, used to measure the HSQ profile for simulations.

3.4. Discussion

In the limit of weak absorption (waveguide dominated losses), the maximum sensitivity is achieved with a waveguide of length $1/\alpha$, where α is the waveguide loss in cm^{-1}, meaning that with 1 dB/cm losses a waveguide length of 4.34 cm will provide optimal sensitivity. We have previously demonstrated losses in 4 μm wide waveguides in TE polarisation of ~ 1 dB/cm [22]. An optical overlap of ~ 1.2 % therefore provides an interaction length of ~ 520 μm. As an example, we evaluate the requirements for an ammonia sensing system based on the measurements presented here. Ammonia has strong absorption peaks ~ 9.545 μm wavelength, and when detected on the breath, it can be used to diagnose chronic kidney disease [26]. Typically, this requires detection of ammonia in concentrations as low as 400 ppb for healthy individuals [26]. Assuming the losses demonstrated previously [22] of ~ 1 dB/cm for 4 μm waveguides in TE polarisation, and the corresponding optical overlap of 1.2 %, the requirements on the source and detector can be calculated as shown in [27]. For ~ 400 ppb detection of ammonia (absorption cross section of $2.78\text{x}10^{-18}$ cm^2 at ~ 9.545 μm [28]), using our waveguides, a

Optics EXPRESS

detector noise-equivalent-power (NEP) of $4x10^{-9}$ W $Hz^{-0.5}$ is required, with a 50 mW source, and 100 ms integration time, with an SNR of 3. This level of NEP would allow the use of a non-cryogenically cooled detector. Breath analysis techniques are not standardised, and can vary between real-time analysis and techniques where the breath is stored locally and subsequently measured [29]. There are numerous examples of breath analysis for medical diagnostics where an exhalation of 10 s is required; an integration time of 100 ms therefore seems reasonable to provide approximately 100 data points from a single exhalation, which could be further averaged with multiple breaths.

A number of sensing applications could involve proteins or molecules coating the waveguide surface [30]; applications where the evanescent tail could extend beyond the analyte. To give an indication of the performance of such measurements, the optical overlap was calculated within a bounding box, approximated as a thin film coating the waveguide, for a range of thicknesses. The integrated power overlap as a function of the film thickness is demonstrated in Fig. 6, for both TE and TM polarisations. This was calculated for rib-waveguide widths of 3, 4 and 5 μm at a wavelength of 9.55 μm, which is in the spectral vicinity of vibrational modes from bonds in DNA [31]. The simulation assumes that the film is conformal, and coats the waveguide sidewalls and the top surface. For TE modes, and 3 μm wide waveguides, a 50 nm thick conformal film would have approximately a 0.5 % overlap with the optical mode. This is a conservative estimate, as it assumes a film refractive index of n=1.

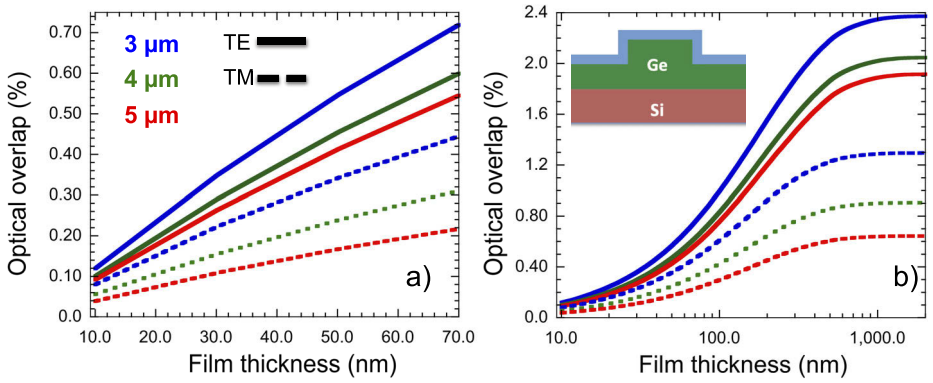

Fig. 6. Simulated modal overlap with a conformal thin film coating a range of rib-waveguides with widths of 3 μm (blue), 4 μm (green) and 5 μm (red), for TE (solid) and TM polarisation (dashed). (a) Shows the optical overlap for films of thicknesses between 10 and 70 nm. (b) Shows optical overlaps of a film up to 2000 nm thick, with a logarithmic scale on the x-axis. The inset shows a schematic of a conformal film (blue) coating a Ge rib waveguide; the region in which the optical power is integrated.

Ultimately, when comparing waveguide platforms, only the loss and the optical overlap with the analyte can be considered. The Ge-on-Si platform is ideally placed to meet these requirements, with low-loss demonstrated previously [22] and an experimentally verified optical overlap of 2 % for the 3 μm waveguides (which will be larger for thicker films). SiGe waveguides have shown excellent low losses, and the material is well suited to engineering non-linear properties [32], however the optical overlap is limited due to graded buffers that pull the mode towards the substrate. Ge-on-SiN platforms have been used to demonstrate sensing in the MIR with spiral waveguides [15], but there have been no demonstrations in the molecular fingerprint regime, where there is strong SiN absorption. This limits the platform to shorter wavelength and therefore prohibits the use of applications where chemical discrimination is required. This work therefore verifies that Ge-on-Si is an excellent candidate for waveguide spectroscopy within the

Optics EXPRESS

molecular fingerprint regime, where broadband low-loss and good optical overlaps can lead to highly sensitive measurements.

Future work will focus on determining the optimal waveguide geometry for sensing in terms of the etch depth of the rib-waveguide. There is likely inherent trade-offs between propagation loss and optical overlap of the analyte. Simulations reveal that in the Ge-on-Si platform, however, the optical power in the air cladding of TE modes has a weak dependence on etch depth, with a slight reduction in overlap with increased etch depth, while TM modes demonstrate the opposite trend. Further considerations in this design choice will involve the achievable bending radius for low loss, and compatibility with optical components such as polarisation rotators.

4. Conclusion

We have demonstrated molecular fingerprint sensing with low loss, single mode Ge-on-Si waveguides, using PMMA and HSQ films. Transmission measurements using bare and coated waveguides allowed the measurement of Si-O-Si vibrations with only a 10 μm region of the waveguide coated. This highlights the advantage of working at wavelengths where these molecular vibrations are resonant. In order to improve the dynamic range of the measurement, a multi-path length approach was demonstrated, with multiple waveguides having different lengths exposed to the analyte. This is a unique feature for waveguide spectroscopy allowing higher dynamic range from a single sample compared to ATR and surface normal FTIR. This, along with broadband low-waveguide losses, are key to spectral identification of analytes in the molecular fingerprint regime. These results therefore demonstrate the potential of the Ge-on-Si platform, for integrated sensing in the MIR, particularly for applications such as blood analysis, or evanescent sensing of DNA or biological samples.

Funding

Engineering and Physical Sciences Research Council (EP/N003225/1); Royal Academy of Engineering (RF\201819\18\187).

Disclosures

The authors declare no conflicts of interest.

References

1. J. M. Hollas, *Modern Spectroscopy* (Wiley, 2004), 4th ed.
2. J. Chou, *Hazardous Gas Monitors: A Practical Guide to Selection, Operation, and Applications* (McGraw-Hill, USA, 2000).
3. E. R. Deutsch, P. Kotidis, N. Zhu, A. K. Goyal, J. Ye, A. Mazurenko, M. Norman, K. Zafiriou, M. Baier, and R. Connors, "Active and passive infrared spectroscopy for the detection of environmental threats," Proc. SPIE **9106**, 91060A (2014).
4. B. Mizaikoff, "Waveguide-enhanced mid-infrared chem/bio sensors," Chem. Soc. Rev. **42**(22), 8683–8699 (2013).
5. J. M. Chalmers, H. G. Edwards, and M. D. Hargreaves, eds., *Infrared and Raman Spectroscopy in Forensic Science* (Wiley, 2012).
6. Y. C. Chang, P. Wägli, V. Paeder, A. Homsy, L. Hvozdara, P. Van Der Wal, J. Di Francesco, N. F. De Rooij, and H. Peter Herzig, "Cocaine detection by a mid-infrared waveguide integrated with a microfluidic chip," Lab Chip **12**(17), 3020–3023 (2012).
7. P. M. Pellegrino, E. L. Holthoff, and M. E. Farrell, eds., *Laser Based Optical Detection of Explosives* (CRC Press, 2017).
8. L. Baldassarre, E. Sakat, J. Frigerio, A. Samarelli, K. Gallacher, E. Calandrini, G. Isella, D. J. Paul, M. Ortolani, and P. Biagioni, "Midinfrared plasmon-enhanced spectroscopy with germanium antennas on silicon substrates," Nano Lett. **15**(11), 7225–7231 (2015).
9. R. Lin, F. Chen, X. Zhang, Y. Huang, B. Song, S. Dai, X. Zhang, and W. Ji, "Mid-infrared optical properties of chalcogenide glasses within tin-antimony-selenium ternary system," Opt. Express **25**(21), 25674–25688 (2017).
10. C. Charlton, M. Giovannini, J. Faist, and B. Mizaikoff, "Fabrication and characterization of molecular beam epitaxy grown thin-film gaas waveguides for mid-infrared evanescent field chemical sensing," Anal. Chem. **78**(12), 4224–4227 (2006).

Optics EXPRESS

11. T. Lewi and A. Katzir, "Silver halide single-mode strip waveguides for the mid-infrared," Opt. Lett. **37**(13), 2733–2735 (2012).
12. J. M. Ramirez, Q. Liu, V. Vakarin, J. Frigerio, A. Ballabio, X. L. Roux, D. Bouville, L. Vivien, G. Isella, and D. Marris-Morini, "Graded SiGe waveguides with broadband low-loss propagation in the mid infrared," Opt. Express **26**(2), 870–877 (2018).
13. A. Osman, M. Nedeljkovic, J. S. Penades, Y. Wu, Z. Qu, A. Z. Khokhar, K. Debnath, and G. Z. Mashanovich, "Suspended low-loss germanium waveguides for the longwave infrared," Opt. Lett. **43**(24), 5997–6000 (2018).
14. A. Malik, S. Dwivedi, L. V. Landschoot, M. Muneeb, Y. Shimura, G. Lepage, J. V. Campenhout, W. Vanherle, T. V. Opstal, R. Loo, and G. Roelkens, "Ge-on-Si and Ge-on-SOI thermo-optic phase shifters for the mid-infrared," Opt. Express **22**(23), 28479–28488 (2014).
15. W. Li, P. Anantha, K. H. Lee, H. D. Qiu, X. Guo, S. C. K. Goh, L. Zhang, H. Wang, R. A. Soref, and C. S. Tan, "Spiral waveguides on germanium-on-silicon nitride platform for mid-IR sensing applications," IEEE Photonics J. **10**(3), 1–7 (2018).
16. K. Gallacher, A. Ballabio, R. W. Millar, J. Frigerio, A. Bashir, I. MacLaren, G. Isella, M. Ortolani, and D. J. Paul, "Mid-infrared intersubband absorption from p-Ge quantum wells grown on Si substrates," Appl. Phys. Lett. **108**(9), 091114 (2016).
17. M. P. Fischer, A. Riede, K. Gallacher, J. Frigerio, G. Pellegrini, M. Ortolani, D. J. Paul, G. Isella, A. Leitenstorfer, P. Biagioni, and D. Brida, "Plasmonic mid-infrared third harmonic generation in germanium nanoantennas," Light: Sci. Appl. **7**(1), 106 (2018).
18. D. J. Paul, K. Gallacher, R. W. Millar, V. Giliberti, E. Calandrini, L. Baldassarre, M. P. Fischer, J. Frigerio, A. Ballabio, E. Sakat, G. Pellegrini, D. Brida, G. Isella, M. Ortolani, and P. Biagioni, "n-Ge on Si for mid-infrared plasmonic sensors," in *2017 IEEE Photonics Society Summer Topical Meeting Series (SUM)*, (2017), pp. 125–126.
19. E. R. Deutsch, P. Kotidis, N. Zhu, A. K. Goyal, J. Ye, A. Mazurenko, M. Norman, K. Zafiriou, M. Baier, and R. Connors, "Active and passive infrared spectroscopy for the detection of environmental threats," Proc. SPIE **9106**, 91060A (2014).
20. K. Araki, N. Yagi, Y. Ikemoto, H. Yagi, C.-J. Choong, H. Hayakawa, G. Beck, H. Sumi, H. Fujimura, T. Moriwaki, Y. Nagai, Y. Goto, and H. Mochizuki, "Synchrotron FTIR micro-spectroscopy for structural analysis of lewy bodies in the brain of parkinson's disease patients," Sci. Rep. **5**(1), 17625 (2015).
21. V. Mittal, M. Nedeljkovic, L. G. Carpenter, A. Z. Khokhar, H. M. H. Chong, G. Z. Mashanovich, P. N. Bartlett, and J. S. Wilkinson, "Waveguide absorption spectroscopy of bovine serum albumin in the mid-infrared fingerprint region," ACS Sens. **4**(7), 1749–1753 (2019). PMID: 31264410.
22. K. Gallacher, R. Millar, U. Griškevičiūte, L. Baldassarre, M. Sorel, M. Ortolani, and D. J. Paul, "Low loss Ge-on-Si waveguides operating in the 8 - 14 μm atmospheric transmission window," Opt. Express **26**(20), 25667–25675 (2018).
23. M. M. Mirza, H. Zhou, P. Velha, X. Li, K. E. Docherty, A. Samarelli, G. Ternent, and D. J. Paul, "Nanofabrication of high aspect ratio (~50:1) sub-10 nm silicon nanowires using inductively coupled plasma etching," J. Vac. Sci. Technol., B: Microelectron. Nanometer Struct.–Process., Meas., Phenom. **30**(6), 06FF02 (2012).
24. Y. Han, L. Han, Y. Yao, Y. Li, and X. Liu, "Key factors in FTIR spectroscopic analysis of DNA: the sampling technique, pretreatment temperature and sample concentration," Anal. Methods **10**(21), 2436–2443 (2018).
25. S. Choi, M. J. Word, V. Kumar, and I. Adesida, "Comparative study of thermally cured and electron-beam-exposed hydrogen silsesquioxane resists," J. Vac. Sci. Technol. B **26**(5), 1654–1659 (2008).
26. S. Davies, P. Spanel, and D. Smith, "Quantitative analysis of ammonia on the breath of patients in end-stage renal failure," Kidney Int. **52**(1), 223–228 (1997).
27. Q. Liu, J. M. Ramirez, V. Vakarin, X. Le Roux, A. Ballabio, J. Frigerio, D. Chrastina, G. Isella, D. Bouville, L. Vivien, C. A. Ramos, and D. Marris-Morini, "Mid-infrared sensing between 5.2 and 6.6 μm wavelengths using Ge-rich SiGe waveguides [Invited]," Opt. Mater. Express **8**(5), 1305 (2018).
28. S. Sharpe, R. Sams, and T. Johnson, "The PNNL quantitative IR database for infrared remote sensing and hyperspectral imaging," in *Applied Imagery Pattern Recognition Workshop, 2002. Proceedings.*, vol. 2002, January (IEEE Comput. Soc, 2002), pp. 45–48.
29. O. Lawal, W. M. Ahmed, T. M. E. Nijsen, R. Goodacre, and S. J. Fowler, "Exhaled breath analysis: a review of 'breath-taking' methods for off-line analysis," Metabolomics **13**(10), 110 (2017).
30. M. Kazmierczak, J. Flesch, J. Mitzloff, G. Capellini, W. M. Klesse, O. Skibitzki, C. You, M. Bettenhausen, B. Witzigmann, J. Piehler, T. Schroeder, and S. Guha, "Stable and selective self-assembly of α-lipoic acid on Ge(001) for biomolecule immobilization," J. Appl. Phys. **123**(17), 175305 (2018).
31. M. L. S. Mello and B. C. Vidal, "Changes in the infrared microspectroscopic characteristics of dna caused by cationic elements, different base richness and single-stranded form," PLoS One **7**(8), e43169 (2012).
32. J. Frigerio, A. Ballabio, C. Ciano, A. Mancini, L. Baldassarre, J. Allerbeck, J. Kuttruff, G. Isella, D. Brida, M. Virgilio, and M. Ortolani, "Ge/SiGe asymmetric quantum wells for second harmonic generation in the mid-infrared," in *2019 Conference on Lasers and Electro-Optics Europe and European Quantum Electronics Conference*, (Optical Society of America, 2019), p. cd p 7.